

Unexplored reactivity of $(S_n)^{2-}$ Oligomers with transition metals in low-temperature solid-state reactions

Shunsuke Sasaki, Melanie Lesault, Elodie Grange, Etienne Janod, Benoît Corraze, Sylvian Cadars, Maria Teresa Caldes, Catherine Guillot-Deudon, Stéphane Jobic and Laurent Cario**

Institut des Matériaux Jean Rouxel (IMN), Université de Nantes, CNRS, 2 rue de la Houssinière, BP 32229, 44322 Nantes Cedex 3, France.

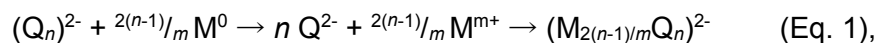
*E-mail. Stephane.Jobic@cnrs-imn.fr, Laurent.Cario@cnrs-imn.fr

ABSTRACT

Chalcogenides (Q = S, Se, Te), one of the most important family of materials in solid-state chemistry, differ from oxides by their ability to form covalently-bonded $(Q_n)^{2-}$ oligomers. Each chalcogen atom within such entity fulfills the octet rule by sharing electrons with other chalcogen atoms but some antibonding levels are vacant. This makes these oligomers particularly suited for redox reactions in solid state, namely towards elemental metals with a low redox potential that may be oxidized. We recently used this strategy to design, at low temperature and in an orientated manner, materials with 2D infinite layers through the topochemical insertion of copper into preformed precursors containing $(S_2)^{2-}$ and/or $(Se_2)^{2-}$ dimers (*i.e.* $La_2O_2S_2$, $Ba_2F_2S_2$ and $LaSe_2$). Herein we extend the validity of the concept to the redox activity of $(S_2)^{2-}$ and $(S_3)^{2-}$ oligomers towards 3d transition metal elements (Cu, Ni, Fe) and highlight the strong relationship between the structures of the precursors, BaS_2 and BaS_3 , and the products, $BaCu_2S_2$, $BaCu_4S_3$, $BaNiS_2$ and $BaFe_2S_3$. Clearly, beyond the natural interest for the chemical reactivity of oligomers to generate compounds, this soft chemistry route may conduct to the rational conception of materials with a predicted crystal structure.

Chalcogenides has been established as one of the most important field in solid-state chemistry, owing to the richness of their chemical compositions, the complexity of their structural arrangements and their numerous applications (e.g. solar cells,¹ thermoelectricity,² non-volatile memories³). Sulfides, selenides, and tellurides received also much attention for their electronic instabilities,⁴ and were recently spotlighted for their optical and electronic properties when prepared as two-dimensional nanosheets.⁵⁻⁶ From a chemical point of view, the uniqueness of chalcogenides compared to oxides arises from their ability to stabilize a large series of discrete Q_n oligomers or infinite polymerized Q_n network.⁷⁻⁹ The reactive flux method led, for example, to the stabilization of a myriad of new materials with a large variety of Q_n oligomers (n up to ca. 10) that may coexist in the same framework.¹⁰ The occurrence of these Q-Q bonds affect drastically the electronic structure and therefore the physical properties¹¹⁻¹³ of the materials in which they are embedded.¹⁴⁻¹⁶ But the presence of Q-Q bonds also confers on these materials a remarkable chemical reactivity in the solid state.¹⁷⁻²⁰ In that respect, we recently demonstrated that the redox activity of $(Q_2)^{2-}$ pairs ($Q = S, Se$) could be valuable to design and synthesize layered transition metal chalcogenides in a topochemical manner.²¹ We found that the low-temperature solid-solid reactions between elemental copper and precursors containing $(Q_2)^{2-}$ pairs sandwiched between redox-inactive cationic layers trigger the formation of layered quaternary and ternary compounds thanks to the insertion of copper and the Q-Q bond cleavage.

Notably, this novel topochemical route can be written in a general way as follows:



where M = transition metal and $Q = S, Se, Te$.

Accordingly, it should work with various transition metals and low-dimensional polychalcogenides species as long as the electron transfer from the metal to the oligomer is feasible (see Fig. 1a). It holds therefore the promise to become a versatile synthetic methodology to explore novel transition metal chalcogenides with unconventional properties and a low dimensional structure inherited from the precursor (see Fig. 1b). To evidence such a general applicability, we showcase the reactivity of BaS_2 and BaS_3 with $(S_2)^{2-}$ dimer and $(S_3)^{2-}$ trimers towards the insertion of copper, nickel or iron. In particular, we demonstrate the ability of the method to stabilize, in soft conditions, $BaNiS_2$, a promising material for spintronic due to its Rashba spin-orbit coupling,²² and $BaFe_2S_3$, the first spin-ladder iron-based superconductor.²³

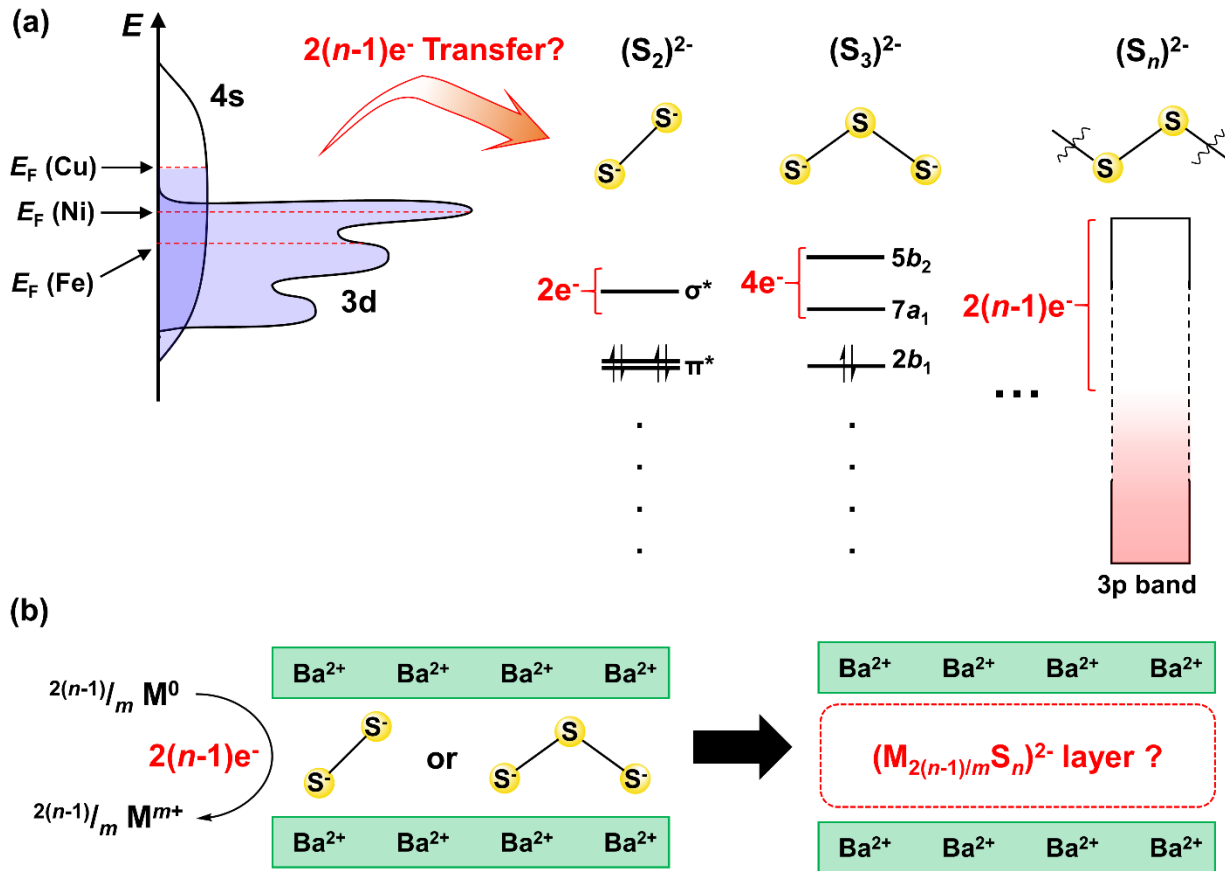


Fig. 1. (a) Schematic energy diagram of the redox chemistry between transition metals and sulfur oligomers. The simplistic density of states depicting band filling of 3d metals is adapted from reference 24. (b) Insertion of transition metals triggered by the redox reaction with polychalcogenides leading to the creation of a two-dimensional transition metal chalcogenide layer sandwiched between "inert" cationic layers.

Barium sulfides are known to exhibit several polysulfide species BaS_n ($n = 2 - 5$) although tetramers and pentamers are very difficult to isolate.²⁵ Herein BaS_2 and BaS_3 have been chosen to examine the reactivity of $(S_2)^{2-}$ and $(S_3)^{2-}$ oligomers towards Cu, Ni and Fe. BaS_2 (SG: $C2/c$) and BaS_3 (SG: $P-42_1m$) materials can be regarded as the 2D assembly of $(S_2)^{2-}$ or $(S_3)^{2-}$ discrete entities that alternate along the stacking axis with Ba^{2+} cationic layers (Fig. 2a, b). Intramolecular S-S distances are 2.12 Å for $(S_2)^{2-}$ dimers and 2.08 Å for $(S_3)^{2-}$ trimers,²⁶ corresponding to typical values for S-S single bonds.²⁷ As calculated in our previous report,²⁸ such $(S_2)^{2-}$ dimers feature molecular orbitals common to homoatomic dimers of p-block elements (Fig. 1a). In the same way our DFT calculation of BaS_3 demonstrates that its density of states are characterized clearly by molecular orbitals of $(S_3)^{2-}$ trimers, which accord well with the electronic structure of the isolated

S₃ molecule (Fig. S1).²⁹ Accordingly, BaS₂ and BaS₃ should be able to accommodate up to 2 and 4 donated electrons per formula unit to yield the closed shell S²⁻ species.

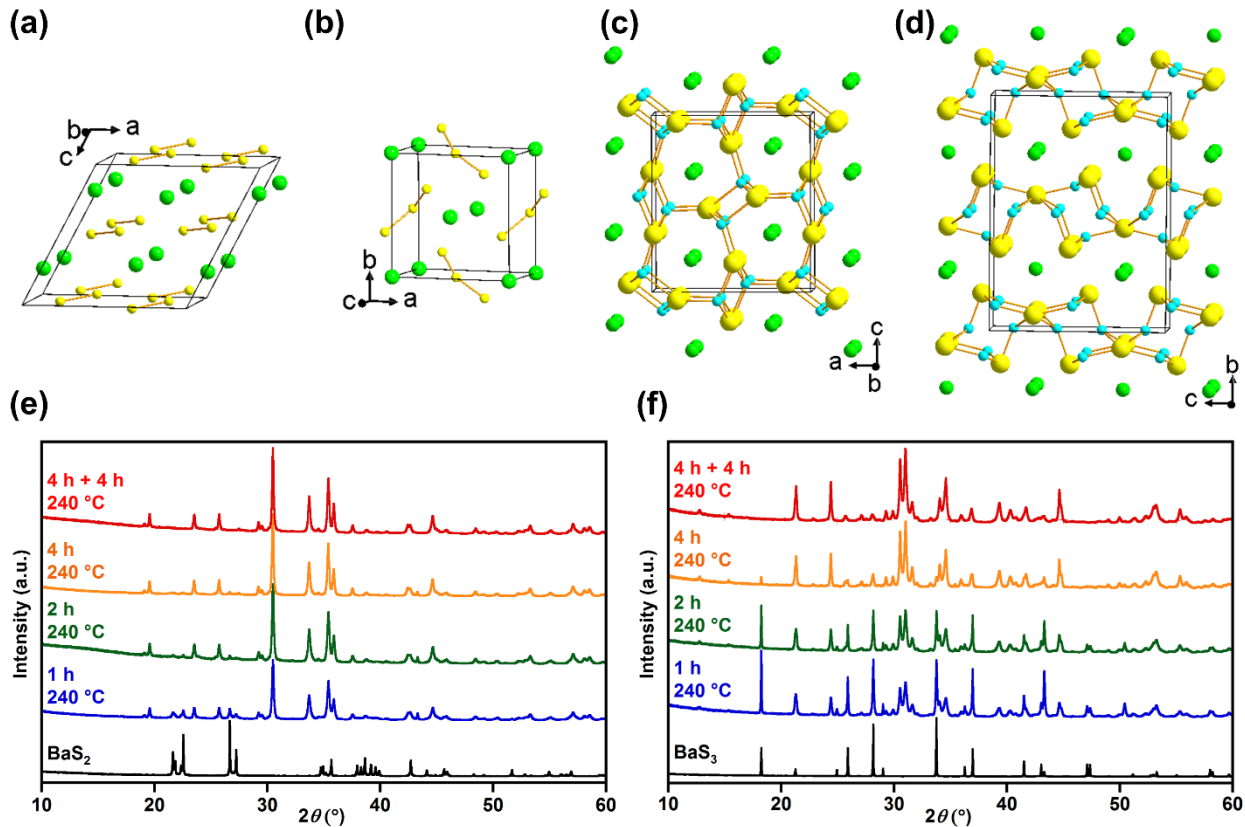


Fig. 2. Structures of (a) BaS₂, (b) BaS₃, (c) α -BaCu₂S₂ and (d) β -BaCu₄S₃. Barium, copper and sulfur atoms are represented by lime, cyan and yellow spheres. (e), (f) XRD patterns of the BaS₂ + 2Cu and BaS₃ + 4Cu mixtures after the thermal treatments at 240 °C for 1, 2, 4 and 4 + 4 h, respectively, respectively.

Let us first consider the incorporation of Cu into BaS₂ and BaS₃. Following Eq. 1, the BaS₂:Cu = 1:2 (mol/mol) mixture was heated at low temperature in a sealed pyrex tube to initiate the insertion of copper in the host lattice. Indeed, X-ray diffraction (XRD) evidenced that peaks of the BaS₂ precursor disappeared within few hours at 240 °C while new peaks concomitantly emerged (Fig. 2e, See Fig. S2-S3 for the detail) that were all assigned to α -BaCu₂S₂ (SG: Pnma) (Fig. 2c),³⁰ i.e. the low-temperature form known to convert into the high-temperature form (β -BaCu₂S₂, SG: I4/mmm) above 540 °C.³¹ In particular, after annealing at 240 °C for 4h subsequent to a manual milling step, pure BaCu₂S₂ was obtained. The same synthesis route was applied to the BaS₃:Cu = 1:4 (mol/mol) mixture. The heating at low temperature quickly triggers the conversion of BaS₃ into BaCu₄S₃ (Fig. 2d), again without detection of intermediates or impurity

phases (Fig. 2f, See Fig. S4 for the detail). According to our Rietveld analysis (See Table S2, Fig. S5 and S6), conversion of BaS_3 into BaCu_4S_3 was slower than BaS_2 into BaCu_2S_2 . Moreover, unlike the synthesis of BaCu_2S_2 , BaCu_4S_3 was obtained as two polymorphs; the molar ratio between the low-temperature phase (α phase) and the high-temperature one (β phase) being equal to *ca.* 2 : 3 regardless the duration of the heating treatment (Fig. S7). The two polymorphs turn out to be structurally very similar, the β - (SG: Cmc_m, Fig. 2d) and α - (SG: Pnma) phase exhibiting flat and corrugated Ba^{2+} and Cu^+ layers, respectively.³² Since its reaction temperature ($T = 240^\circ\text{C}$) was far lower than the $\alpha \rightarrow \beta$ phase transition temperature of $640 \pm 10^\circ\text{C}$,³² β phase was formed as a metastable compound. This fact supports the practicability of our soft chemistry route as a novel tool to explore metastable phases. Also Raman peaks ascribed to the normal modes of $(\text{S}_2)^{2-}$ dimers³³⁻³⁴ in BaS_2 and $(\text{S}_3)^{2-}$ trimers³⁵ in BaS_3 have disappeared in the course of the reaction with copper (Fig. S8) while photoluminescence of the products masked small Raman signals. In any case, these synthesis results with BaS_2 and BaS_3 as precursors clearly demonstrate the redox activity of not only $(\text{S}_2)^{2-}$ dimers but also $(\text{S}_3)^{2-}$ trimers towards the insertion of copper. This type of intercalation reactions is likely to occur with other oligomers and might also explain the stabilization of KCu_4S_3 via heating of a $\text{K}_2\text{S}_5 + \text{Cu}$ mixture while K_2S_5 used as a flux was not yet melted.³⁶

So far, the reactivity of metal towards holes at empty antibonding levels of $(\text{S}_n)^{2-}$ polysulfides has been spotlighted for copper only.²¹ Herein we examine the reactivity of $(\text{S}_n)^{2-}$ oligomers toward open-shell 3d transition metals, namely Ni and Fe, whose work functions are comparable with copper (Ni (5.2 eV) > Cu (4.64 eV) > Fe (4.5 eV)³⁷ but stable as divalent cations in chalcogenides.

Practically, Ni was initially mixed to BaS_2 in 1:1 ratio, and then heated at 340°C for 12 h (see SI for details). The powder XRD pattern (Fig. 3b) displayed then relatively broad peaks unambiguously assigned to BaNiS_2 ³⁸ besides sharp peaks due to BaS and NiS present in 31 wt% and 28 wt%, respectively (see Table S3 and Fig. S9 for Rietveld refinement). Clearly, the decomposition of BaS_2 into BaS severely competed with the insertion of Ni. Indeed this parasitic reaction was bypassed by introducing a $\text{BaS}_3:\text{Ni} = 1:2$ mixture into the preheated furnace and subsequent annealing for 1h. The obtained XRD pattern indicates much better $\text{BaNiS}_2:\text{BaS}$ molar ratio up to 89:11. Our follow-up experiment revealed the reaction of Ni with BaS_3 first lead to the decomposition into BaS_2 and NiS_x species (see Fig. S10 for details). Then remaining Ni intercalates into the BaS_2 produced in situ, which is likely stabilized by the sulfur vapor pressure built in the sealed tube. The reaction between BaS_3 and Fe suffered also from the decomposition into BaS and FeS , and such decomposition was suppressed using a similar heating treatment (Fig

3d). Introduction of the mixture into a preheated furnace followed by annealing at 340 °C for 1h yielded BaFe_2S_3 ³⁹ at 91 wt% with FeS and $\text{Ba}_6\text{Fe}_8\text{S}_{15}$ as very minor phases (See Fig. S11 for Rietveld refinement).

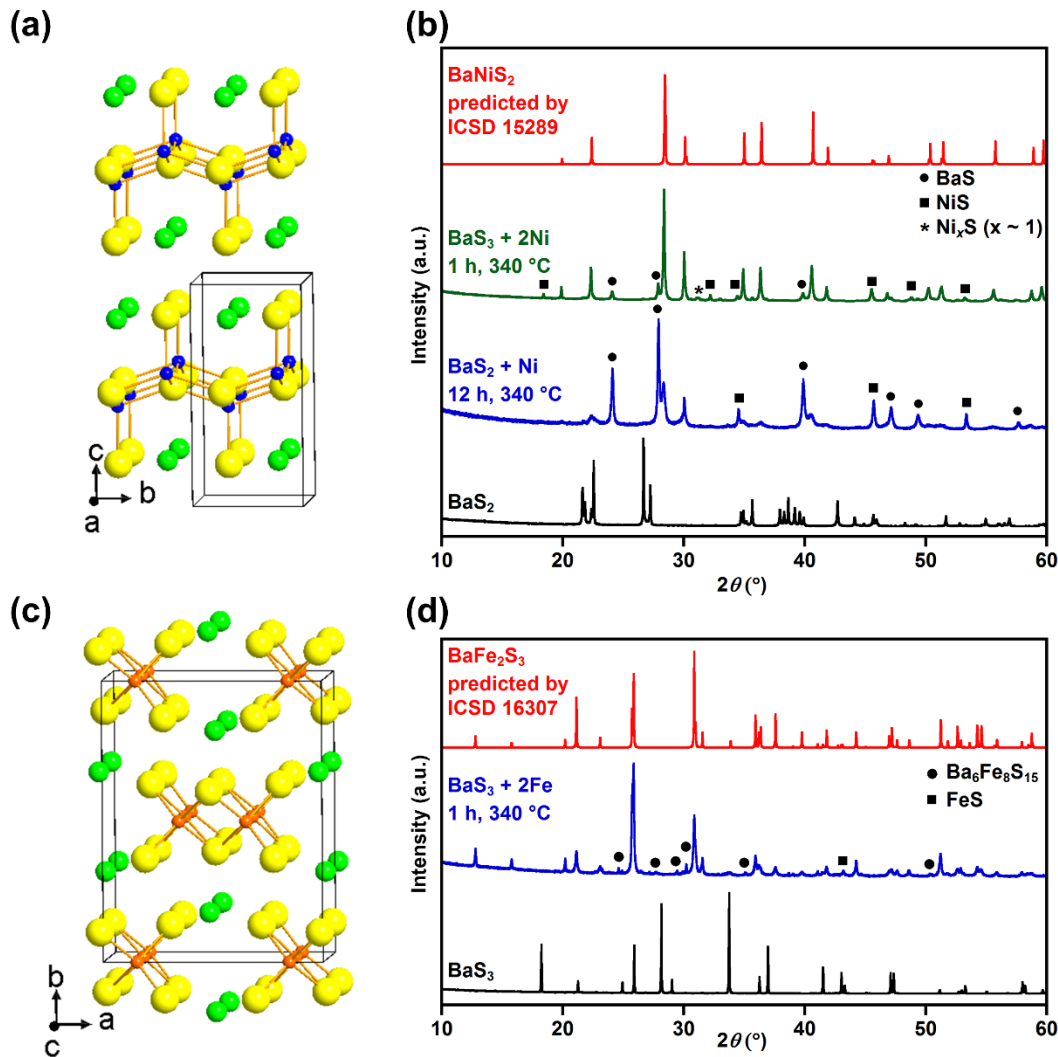


Fig. 3. (a) Structure of BaNiS_2 ; (b) theoretical XRD pattern of BaNiS_2 (red), experimental XRD pattern of the $\text{BaS}_3 + 2\text{Ni}$ (green) and the $\text{BaS}_2 + \text{Ni}$ (blue) mixture after thermal treatment at 340 °C for 1 and 12 h, respectively, as well as XRD pattern of BaS_2 (black). (c) Structure of BaFe_2S_3 ; (b) theoretical XRD pattern of BaFe_2S_3 (red), experimental XRD pattern of a $\text{BaS}_3 + 2\text{Fe}$ mixture after the thermal treatment at 340 °C for 1 h (blue), and XRD pattern of BaS_3 (black).

These results demonstrate that the open-shell 3d transition metals (e.g. Ni^{2+} and Fe^{2+} in square-pyramidal and tetrahedral sites, respectively) can be inserted into $(\text{S}_n)^{2-}$ containing precursors at temperatures ($T = 340\text{ }^\circ\text{C}$) much lower than the ones ($T > 800\text{ }^\circ\text{C}$) needed for conventional ceramic routes for BaNiS_2 and BaFe_2S_3 .³⁹⁻⁴¹

In our previous report,²¹ insertion of copper into $(\text{S}_2)^{2-}$ containing materials were shown to be topochemical. The same observation is made here as demonstrated below for BaNiS_2 and BaFe_2S_3 (Fig. 2f and 3d). The hypothetical topochemical reaction pathway for BaCu_4S_3 is also given in Fig. S12.

In BaS_2 (SG: $\text{C2}/c$), the $(\text{S}_2)^{2-}$ dimers occupy distorted octahedral sites of Ba^{2+} . In the case of $\text{BaS}_2 \rightarrow \text{BaNiS}_2$ transformation, small atomic rearrangement like the splitting of the dimers and concomitant separation of the basal planes of the Ba_6 octahedra are sufficient to reach the Ba-S framework of BaNiS_2 structure type. This creates a corrugated sulfur atomic layer that can then accommodate Ni^{2+} cations (Fig. 4). Preservation of the structural building blocks and of the layered structure asserts the topochemical nature of the process.

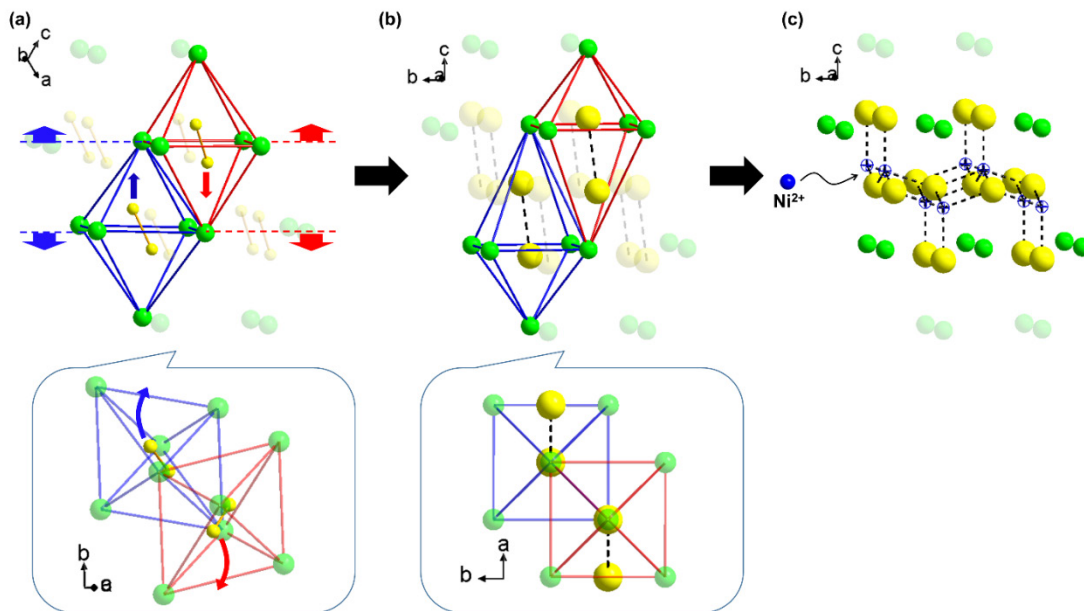


Fig. 4. Plausible reaction pathway from BaS_2 to BaNiS_2 . (a) Structure of BaS_2 . Two differently distorted octahedra of Ba_6S_2 are colored in red and blue, respectively (Inset: projection of these two octahedra on their basal planes). (b) Structure of BaNiS_2 , represented without the Ni atoms, highlighting the elongated Ba_6 octahedra and broken S-S pairs. (c) Structure of BaNiS_2 signifying the square-pyramidal sites for Ni^{2+} cations and Ni-S bonds by blue hollow spheres and broken lines, respectively.

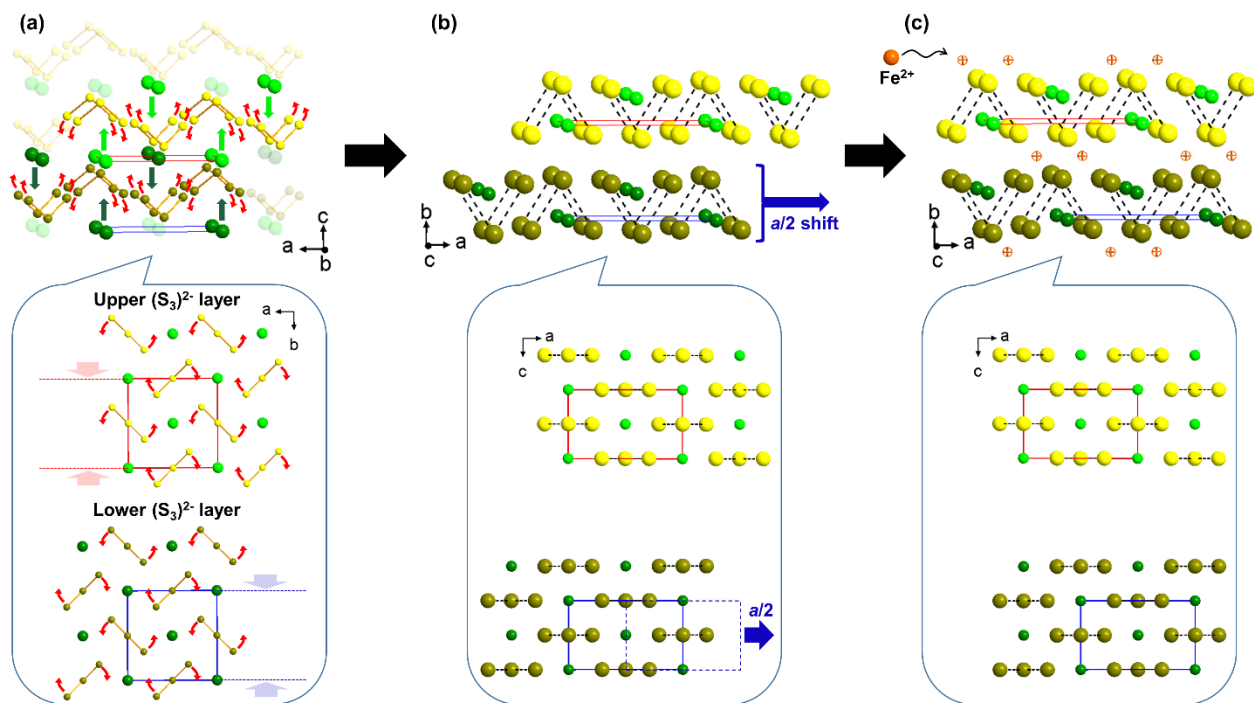


Fig. 5. Plausible reaction pathway from BaS₃ to BaFe₂S₃. A red or blue arrow describe movement of each structural unit. (a) Structure of BaS₃. Ba²⁺ cations colored lime/deep green are merged into upper/lower (S₃)²⁻ double layers colored yellow/brown, respectively. Concomitant S-S bond breaking leads (b) a hypothetical structure before the transformation to reach the structure of BaFe₂S₃ through *a*/2 shift of bottom ^{2/∞}[BaS₃] layer. (c) Structure of BaFe₂S₃ displaying tetrahedral sites for Fe²⁺ cations by orange hollow spheres.

In BaS₃ (SG: *P*-421*m*), a double layer made of two columns of (S₃)²⁻ trimers is sandwiched within a base-centered sub-lattice of Ba²⁺. In the case of BaS₃ → BaFe₂S₃ transformation, the conformational change of the broken trimers and concomitant segregation of Ba²⁺ cations forms a [BaS₃]²⁻ layer with the same framework as observed in the BaFe₂S₃ structure type (Fig. 5). The iron intercalation process occurs therefore between two successive [BaS₃]²⁻ layers achieved through slight reorganization of the BaS₃ framework.

In both BaNiS₂ and BaFe₂S₃ cases the structural transformation from the precursor occurs without destructive reorganization of the precursor framework, which explains the low energy costs of the reactions. It supports an underlying topochemical nature of the processes as already observed in our previous study.

To sum up, we demonstrated the low-temperature reactivity of compounds containing (S_{*n*})²⁻ (*n* = 2-3) oligomers, *i.e.* BaS₂ and BaS₃, towards transition metals to give BaCu₂S₂, BaCu₄S₃, BaNiS₂ and BaFe₂S₃ retaining their original structural motif. These reactions can be regarded as

a thermo-assisted intercalation process involving the diffusion of the transition metal from the surface to the precursor bulk and the concomitant cleavage of S-S bonds thanks to electron transfer from the metal. The potential of this novel soft chemistry route for inorganic solids is tremendous according to the large number of precursors containing chalcogenide oligomers and might lead to the discovery of layered transition metal chalcogenides with remarkable properties.

ACKNOWLEDGEMENTS

The authors thank P.-E. Petit and J.-Y. Mevellec in IMN for their help on X-ray diffraction measurements and Raman spectroscopy, respectively. S.S. is financially supported by JSPS Overseas Research Fellowships.

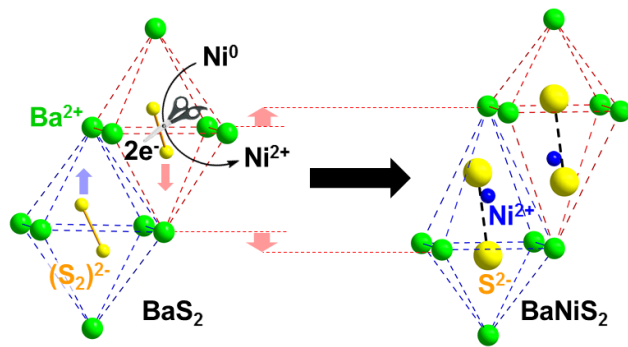
REFERENCES

1. Aldakov, D.; Lefrançois, A.; Reiss, P. Ternary and Quaternary Metal Chalcogenide Nanocrystals: Synthesis, Properties and Applications. *J. Mater. Chem. C* **2013**, *1*, 3756-3776.
2. Tan, G.; Zhao, L.-D.; Kanatzidis, M. G. Rationally Designing High-Performance Bulk Thermoelectric Material. *Chem. Rev.* **2016**, *116*, 12123-12149.
3. Cario, L.; Vaju, C.; Guiot, V.; Janod, E. Electric - Field - Induced Resistive Switching in a Family of Mott Insulators: Towards a New Class of RRAM Memories. *Adv. Mater.* **2010**, *22*, 5193-5197.
4. Monceau, P. Charge Density Wave Transport in Transition Metal Tri- and Tetra-chalcogenides. In *Electronic Properties of Inorganic Quasi-One-Dimensional Compounds: Part II — Experimental*; Monceau, P., Ed.; D. Reidel Publishing Company: Holland, **1985**; p139.
5. Wang, Q. H.; Kalantar-Zadeh, K.; Kis, A.; Coleman, J. N.; Strano, M. S. Electronics and Optoelectronics of Two-Dimensional Transition Metal Dichalcogenides. *Nat. Nanotech.* **2012**, *7*, 699-712.
6. Butler, S. Z.; Hollen, S. M.; Cao, L.; Cui, Y.; Gupta, J. A.; Gutiérrez, H. R.; Heinz, T. F.; Hong, S. S.; Huang, J.; Ismach, A. F.; Halperin, E.J.; Kuno, M.; Plashnitsa, V. V.; Robinson, R. D.; Ruoff, R. S.; Salahuddin, S.; Shan, J.; Shi, L.; Spencer, M. G.; Terrones, M.; Windl, W.; Goldberger, J. E. Progress, Challenges, and Opportunities in Two-Dimensional Materials beyond Graphene. *ACS Nano* **2013**, *7*, 2898-2926.

7. Jobic, S.; Brec, R.; Rouxel, J. Occurrence and Characterization of Anionic Bondings in Transition Metal Dichalcogenides. *J. Alloys Compd.* **1992**, *178*, 253-283.
8. Brostigen, G.; Kjekshus, A. On the Relationships between the Structure Types Pyrite, Marcasite, and Arsenopyrite. *Acta Chem. Scand.* **1970**, *24*, 2983-2992.
9. Rouxel, J. Low-Dimensional Solids: an Interface between Molecular and Solid-State Chemistry? The Example of Chainlike Niobium and Tantalum Chalcogenides. *Acc. Chem. Res.* **1992**, *25*, 328-336.
10. Kanatzidis, M. G. Discovery-Synthesis, Design, and Prediction of Chalcogenide Phases. *Inorg. Chem.* **2017**, *56*, 3158-3173.
11. Chung, D.-Y.; Jobic, S.; Hogan, T.; Kannewurf, C. R.; Brec, R.; Rouxel, J.; Kanatzidis, M. G. Oligomerization Versus Polymerization of Te_x^{n-} in the Polytelluride Compound BaBiTe_3 . Structural Characterization, Electronic Structure, and Thermoelectric Properties. *J. Am. Chem. Soc.* **1997**, *119*, 2505–2515.
12. Li, Q.; Lin, W.; Yan, J.; Chen, X.; Gianfrancesco, A. G.; Singh, D. J.; Mandrus, D.; Kalinin, S. V.; Pan, M. Bond Competition and Phase Evolution on the IrTe_2 Surface. *Nat. Commun.* **2014**, *5*, 5358.
13. Pascut, G. L.; Haule, K.; Gutmann, M. J.; Barnett, S. A.; Bombardi, A.; Artyukhin, S.; Birol, T.; Vanderbilt, D.; Yang, J. J.; Cheong, S.-W.; Kiryukhin, V. Dimerization-Induced Cross-Layer Quasi-Two-Dimensionality in Metallic IrTe_2 . *Phys. Rev. Lett.* **2014**, *112*, 086402.
14. Rouxel, J. Anion–Cation Redox Competition and the Formation of New Compounds in Highly Covalent Systems. *Chem. Eur. J.* **1996**, *2*, 1053-1059.
15. Schöllhorn, R. From Electronic/Ionic Conductors to Superconductors: Control of Materials Properties. *Angew. Chem. Int. Ed. Engl.* **1988**, *27*, 1392-1400.
16. Schramm, W.; Schöllhorn, R.; Eckert, H.; Müller-Warmuth, W. Nonstoichiometric Channel Chalcogenides $\text{Ti}_x\text{V}_5\text{S}_8$: Topotactic Redox Reactions and NMR studies. *Mater. Res. Bull.* **1983**, *18*, 1283-1289.
17. Luo, K.; Roberts, M. R.; Hao, R.; Guerrini, N.; Pickup, D. M.; Liu, Y.-S.; Edström, K.; Guo, J.; Chadwick, A. V.; Duda, L. C.; Bruce, P. G. Charge-Compensation in 3d-Transition-Metal-Oxide Intercalation Cathodes through the Generation of Localized Electron Holes on Oxygen. *Nat. Chem.* **2016**, *8*, 684-691.
18. Grimaud, A.; Hong, W. T.; Shao-Horn, Y.; Tarascon, J.-M. Anionic Redox Processes for Electrochemical Devices. *Nat. Mater.* **2016**, *15*, 121–126.

19. Li, X.; Qiao, Y.; Guo, S.; Xu, Z.; Zhu, H.; Zhang, X.; Yuan, Y.; He, P.; Ishida, M.; Zhou, H. Direct Visualization of the Reversible O^{2-} / O^- Redox Process in Li-Rich Cathode Materials. *Adv. Mater.* **2018**, *30*, 1705197.
20. Lindic, M. H.; Martinez, H.; Benayad, A.; Pecquenard, B.; Vinatiera, P.; Levasseura, A.; Gonbeau, D. XPS Investigations of TiO_xS_z Amorphous Thin Films used as Positive Electrode in Lithium Microbatteries. *Solid State Ionics* **2005**, *176*, 1529-1537.
21. Sasaki, S.; Driss, D.; Grange, E.; Mevellec, J.-Y.; Caldes, M. T.; Deudon, C. G.; Cadars, S.; Corraze, B.; Janod, E.; Jobic, S.; Cario, L. A Topochemical Approach to Synthesize Layered Materials Based on the Redox Reactivity of Anionic Chalcogen Dimers. *Angew. Chem. Int. Ed.* **2018**, *57*, 13618-13623.
22. Santos-Cottin, D.; Casula, M.; Lantz, G.; Klein, Y.; Petaccia, L.; Le Fèvre P.; Bertran, F.; Papalazarou, E.; Marci, M.; Gauzzi, A. Rashba Coupling Amplification by a Staggered Crystal Field. *Nat. Commun.* **2016**, *7*, 11258.
23. Takahashi, H.; Sugimoto, A.; Nambu, Y.; Yamauchi, T.; Hirata, Y.; Kawakami, T.; Avdeev, M.; Matsubayashi, K.; Du, F.; Kawashima, C.; Soeda, H.; Nakano, S.; Uwatoko, Y.; Ueda Y.; Sato, T. J.; Ohgushi, K. Pressure-Induced Superconductivity in the Iron-Based Ladder Material $BaFe_2S_3$. *Nat. Mater.* **2015**, *14*, 1008-1012.
24. Cullity, B. D. *Introduction to Magnetic Materials*; Wiley: New York, **2009**; p135.
25. Kresse, R.; Baudis, U.; Jäger, P.; Riechers, H. H.; Wagner H.; Winkler, J.; Wolf, H. U. Barium and Barium Compounds. Ullmann's encyclopedia of industrial chemistry **2007**, 621-640.
26. Yamaoka, S.; Lemley, J. T.; Jenks, J. M.; Steinfink, H. Structural Chemistry of the Polysulfides Ba_2S_3 and BaS_3 . *Inorg. Chem.* **1975**, *14*, 129-131.
27. Knop, O.; Boyd, R. J.; Choi, S. C. Sulfur-Sulfur Bond Lengths, or Can a Bond Length be Estimated from a Single Parameter? *J. Am. Chem. Soc.* **1988**, *110*, 7299-7301.
28. Driss, D.; Cadars, S.; Deniard, P.; Mavellec, J.-Y., Corraze, B., Janod, E.; Cario, L. Crystal Structure and Chemical Bonding in the Mixed Anion Compound $BaSF$. *Dalton Trans.* **2017**, *46*, 16244-16250.
29. Morin, M.; Foti, A. E.; Salahub, D. R. Molecular and Electronic Structure of Ozone and Thiozone from LCAO Local Density Calculations. *Can. J. Chem.* **1985**, *63*, 1982-1987.
30. Iglesias, J. E.; Pachali, K. E.; Steinfink, H. Structural Chemistry of Ba_2CdS_3 , Ba_2CdSe_3 , $BaCdS_2$, $BaCu_2S_2$ and $BaCu_2Se_2$. *J. Solid State Chem.* **1974**, *9*, 6-14.
31. Huster, J.; Bronger, W. α - and β - $BaCu_2X_2$ (X = S, Se) - Preparation of Single Crystals in Potassium Chalcogenocyanate Fluxes. *Z. Anorg. Allg. Chem.* **1999**, *625*, 2033-2040.

32. Iglesias, J. E.; Pachali, K. E.; Steinfink, H. The Crystal Structures and Phase Transition of α and β BaCu₄S₃. *Mat. Res. Bull.* **1972**, *7*, 1247-1258.
33. Sourisseau, C.; Cavagnat, R.; Fouassier, M. The Vibrational Properties and Valence Force Fields of FeS₂, RuS₂ pyrites and FeS₂ Marcasite. *J. Phys. Chem. Solids* **1991**, *52*, 537-544.
34. Anastassakis, E.; Perry, C. H. Light Scattering and IR Measurements in XS₂ Pyrite-Type Compounds. *J. Chem. Phys.* **1976**, *64*, 3604-3609.
35. Janz, G. J.; Roduner, E.; Coutts, J. W.; Downey, J. R. Raman Studies of Sulfur-Containing Anions in Inorganic Polysulfides. Barium Trisulfide. *Inorg. Chem.* **1976**, *15*, 1751-1754.
36. Shoemaker, D. P.; Hu, Y. J.; Chung, D. Y.; Halder, G. J.; Chupas, P. J.; Soderholm, L.; Mitchell, J. F.; Kanatzidis, M. G. In Situ Studies of a Platform for Metastable Inorganic Crystal Growth and Materials Discovery. *Proc. Natl. Acad. Sci. U. S. A.* **2014**, *111*, 10922-10927.
37. Michaelson, H. B. The Work Function of the Elements and its Periodicity. *J. Appl. Phys.* **1977**, *48*, 4729-4733.
38. Grey, I. E.; Steinfink, H. Crystal Structure and Properties of Barium Nickel Sulfide, a Square-Pyramidal Nickel(II) Compound. *J. Am. Chem. Soc.* **1970**, *92*, 5093-5095.
39. Hong, H. Y.; Steinfink, H. The Crystal Chemistry of Phases in the Ba-Fe-S and Se Systems. *J. Solid State Chem.* **1972**, *5*, 93-104.
40. Takeda, J.; Sakurai, J.; Nakamura, A.; Kato, M.; Kobayashi, Y.; Sato, M. Thermal Conductivity of BaCo_{1-x}Ni_xS₂. *J. Phys. Soc. Jpn.* **1999**, *68*, 1602-1606.
41. Irizawa, A.; Yoshimura, K.; Kosuge, K. Magnetic and Electrical Properties in BaNiS₂-type Solid Solution. *J. Phys. Soc. Jpn.* **2000**, *69*, 3408-3413.



(For Table of Contents Only)